THE JOURNAL OF PHYSICAL CHEMISTRY C

Article

pubs.acs.org/JPCC

Thermodynamic and Kinetic Analyses of the CO_2 Chemisorption Mechanism on Na_2TiO_3: Experimental and Theoretical Evidences

Pedro Sánchez-Camacho,[†] Issis C. Romero-Ibarra,[†] Yuhua Duan,[‡] and Heriberto Pfeiffer*[,†]

[†]Instituto de Investigaciones en Materiales, Universidad Nacional Autónoma de México, Circuito exterior s/n, Cd. Universitaria, Del. Coyoacán C.P. 04510, México DF, Mexico

[‡]National Energy Technology Laboratory, United States Department of Energy, 626 Cochrans Mill Road, Pittsburgh, Pennsylvania 15236, United States

ABSTRACT: Sodium metatitanate (Na_2TiO_3) was successfully synthesized via a solid-state reaction. The Na_2TiO_3 structure and microstructure were characterized using X-ray diffraction, scanning and transmission electron microscopy, and N_2 adsorption. Then, the CO_2 chemisorption mechanism on Na_2TiO_3 was systematically analyzed to determine the influence of temperature. The CO_2 chemisorption capacity of Na_2TiO_3 was evaluated both dynamically and isothermally, and the products were reanalyzed to elucidate the Na_2TiO_3–CO_2 reaction mechanism. Different chemical species (Na_2CO_3, Na_2O, and $Na_4Ti_5O_{12}$ or $Na_{16}Ti_{10}O_{28}$) were identified during the CO_2 capture process in Na_2TiO_3. In addition, some CO_2 chemisorption kinetic parameters were determined. The $\Delta H^{\ddagger}$ was found to be 140.9 kJ/mol, to the Na_2TiO_3–CO_2 system, between 600 and 780 °C. Results evidenced that CO_2 chemisorption on Na_2TiO_3 highly depends on the reaction temperature. Furthermore, the experiments were theoretically supported by different thermodynamic calculations. The calculated thermodynamic properties of CO_2 capture reactions by (Na_2TiO_3, $Na_4Ti_5O_{12}$, and $Na_{16}Ti_{10}O_{28}$) sodium titanates were fully investigated.

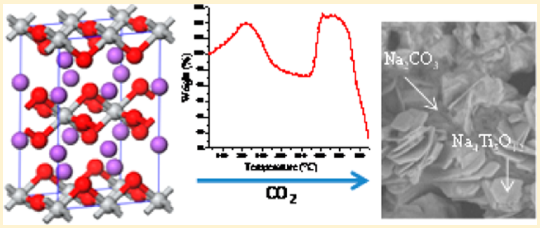

I. INTRODUCTION

Carbon dioxide (CO_2) emissions are one of the most threatening pollution problems in the world. One approach to solve such an environmental problem is CO_2 capture and storage.[1−3] The capture of CO_2 emissions, at stationary point sources (e.g., power stations, smelters, and refineries), is considered a key technology for achieving greenhouse gas reductions. Nevertheless, the selection of the best CO_2 sorbent is not a simple task, as the typical operating temperatures involved are considerably high (500−900 °C), which would rule out the majority of traditional carbon dioxide sorbents, for example, polymer-based membrane materials and amine solution.[4] Therefore, CO_2 capture and storage in solid materials have been considered to be the most practical option as an efficient and cheap alternative to reduce greenhouse gases. In this way, different materials have been proposed as CO_2 captors such as zeolites, porous (active) carbons, metal−organic frameworks (MOFs), alkali metal-promoted alumina and carbonates, alkaline and alkaline-earth ceramics, and layered double hydroxides.[5] These materials are reported to be capable of CO_2 capture at moderate and/or high temperatures.

Among these materials, different alkaline ceramics have been reported as good solid candidates for CO_2 sorbents in terms of large CO_2 sorption capacity and high operating temperatures.[5−79] Some of the alkaline ceramics most studied are lithium silicates (Li_8SiO_6, Li_4SiO_4, and Li_2SiO_3),[6−34] lithium zirconates (Li_8ZrO_6, $Li_6Zr_2O_7$, and Li_2ZrO_3),[32,35−59] lithium aluminate (Li_5AlO_4),[60−63] sodium silicate (Na_2SiO_3),[64] lithium cuprate (Li_2CuO_2),[65−68] and sodium zirconate (Na_2ZrO_3),[69−79] among other ceramics. All these ceramics are able to trap CO_2 chemically, through a similar reaction mechanism: Initially, CO_2 is chemisorbed over the ceramic surface, which implies the formation of an external shell. The external shell is composed of the corresponding alkaline carbonate (Li_2CO_3 or Na_2CO_3) as well as secondary phases and/or metal oxides. Once the superficial external shell is complete, the CO_2 chemisorption can be reactivated if the temperature is increased sufficiently to allow different diffusion processes. Therefore, CO_2 chemisorption is reactivated throughout CO_2 diffusion on mesopore structures (if the external shell contains mesopores)[72] or throughout bulk intercrystalline atomic diffusion processes on these materials.[80]

Alternately, there are several sodium titanates reported in the literature that have been synthesized by different methods[81−83] and used in different applications such as a basic catalyst in transesterification reactions, water splitting reactions, and on different ferroelectric properties.[84−86] However, there is only one report about the use of sodium metatitanate (Na_2TiO_3) as a possible CO_2 captor. López-Ortiz et al.,[79] synthesized and tested different sodium ceramics as CO_2 captors. Sodium metatitanate (Na_2TiO_3) was one of these sodium ceramics, but unfortunately only one CO_2 isothermal experiment was performed at 600 °C. There is not enough information about the CO_2 chemisorption mechanism on sodium titanate,

Received: May 19, 2014
Revised: July 24, 2014
Published: August 7, 2014

dx.doi.org/10.1021/jp504922e | J. Phys. Chem. C 2014, 118, 19822−19832

Na_2TiO_3. The aim of the present work is to systematically analyze the CO_2 chemisorption mechanism on Na_2TiO_3 as a function of temperature. The CO_2 chemisorption capacity of Na_2TiO_3 was evaluated dynamically and isothermally to determine the influence of temperature on the Na_2TiO_3–CO_2 reaction mechanism and kinetic behavior. Additionally, the experiments were theoretically supported by different thermodynamic calculations.

II. EXPERIMENTAL SECTION

Na_2TiO_3 was synthesized via a solid-state reaction. It was obtained by mixing mechanically the corresponding amounts of titanium oxide (TiO_2, Aldrich) and sodium carbonate (Na_2CO_3, Aldrich), with a Na_2CO_3/TiO_2 molar ratio of 1.1:1. Powders were mixed and subsequently calcined at 850 °C for 12 h. After the solid-state synthesis, Na_2TiO_3 was structural and microstructurally characterized, before and after the CO_2 capture process, using powder X-ray diffraction (XRD), scanning (SEM), and transmission (TEM) electron microscopies, and N_2 adsorption–desorption. XRD patterns were obtained with a D8 Bruker diffractometer coupled to a Cu anode X-ray tube in Bragg–Brentano configuration. The $K\alpha_1$ wavelength was selected with a diffracted beam Ge monochromator, and the compounds were identified conventionally using the Joint Committee Powder Diffraction Standards (JCPDS) database. The experimental error was ±3%. Then, Na_2TiO_3 textural characteristics (surface area and porosity) were determined using N_2 adsorption/desorption. For the N_2 adsorption/desorption experiments, the isotherms were acquired on a Bel-Japan Minisorp II at 77 K using a multipoint technique. Previously, the samples were degassed at room temperature for 24 h under vacuum prior to analysis. Scanning and transmission electron microscope images were obtained from JMS-7600F and JEM-1200EX JEOL equipment, respectively. In both cases, the sample preparation was performed by standard procedures.

Different CO_2 chemisorption experiments were performed using Q500HR equipment, from TA Instruments. Initially, Na_2TiO_3 was dynamically heated from room temperature to 850 °C at 5 °C/min. These analyses were carried out under an excess CO_2 atmosphere (Praxair, grade 3.0), using a 60 mL/min of gas flow. A saturated CO_2 atmosphere (100 wt %) was used in order to determine the viability of Na_2TiO_3 as CO_2 captor. For the isothermal analyses, fresh sample was heated at its respective isothermal temperature (between 300 and 700 °C) under a N_2 flow (Praxair, grade 4.8). When the sample reached the corresponding temperature, the gas flow was switched from N_2 to CO_2 (60 mL/min) throughout the duration of the experiment. To elucidate the Na_2TiO_3–CO_2 capture mechanism, products obtained from the isothermal analyses were recharacterized using XRD, SEM, and TEM.

Since the thermodynamic properties of the sodium titanates ($Na_4Ti_5O_{12}$, $Na_{16}Ti_{10}O_{28}$) are not available in the literature, we performed the *ab initio* thermodynamics calculations on these sodium titanates by combining density functional theory (DFT) with lattice phonon dynamics. For comparison reasons, the thermodynamic properties of Na_2TiO_3 were also calculated and compared with the known experimental data. The detailed descriptions of the calculation method can be found in previous studies.[29,87,88] The CO_2 capture reactions of sodium titanate solids can be expressed generically in the form (for convenient description, we normalized the reaction to 1 mol of CO_2)

$$\sum_{Ri} n_{Ri}\mathrm{SolidR}_i + \mathrm{CO_2} \leftrightarrow \sum_{Pj} n_{Pj}\mathrm{SolidP}_j \quad (1)$$

where n_{Ri}, n_{Pj} are the reactants (R_i) and products (P_j) moles involved in the capture reactions. We treat the gas phase CO_2 as an ideal gas. By assuming that the difference between the Gibbs free energy (ΔG°) of the solid phases of reactants (R_i) and products (P_j) can be approximated by the difference in their total energies (ΔE_{DFT}), obtained directly from DFT calculations, and the vibrational free energy of the phonons and by ignoring the PV contribution terms for solids, the variation of the chemical potential ($\Delta\mu$) for reaction 1 with temperature and pressure can be written as

$$\Delta G(T, P) = \Delta G^{\circ}(T) - RT \ln \frac{P_{CO_2}}{P_0} \quad (2)$$

where,

$$\Delta G^{\circ}(T) \approx \Delta E_{DFT} + \Delta E_{ZP} + \Delta F_{PH}(T) - G^{0}_{CO_2}(T) \quad (3)$$

Here, ΔE_{DFT} is the DFT energy difference between the reactants and products of the reaction 1, ΔE_{ZP} is the zero-point energy difference between the reactants and products and can be obtained directly from phonon calculations. ΔF_{PH} is the phonon free energy change excluding zero-point energy (which is already counted into the ΔE_{ZP} term) between the solids of products and reactants. P_{CO_2} is the partial pressure of CO_2 in the gas phase, and P_0 is the standard state reference pressure taken to be 1 bar. The heat of reaction ($\Delta H^{cal}(T)$) can be evaluated through the following equation:

$$\Delta H^{cal}(T) = \Delta G^{\circ}(T) + T[\Delta S_{PH}(T) - S_{CO_2}(T)] \quad (4)$$

where, $\Delta S_{PH}(T)$ is the difference of entropies between product solids and reactant solids. The free energy of CO_2 ($G^0_{CO_2}$) can be obtained from standard statistical mechanics,[87−89] and its entropy (S_{CO_2}) can be found in the empirical thermodynamic databases.[90] First-principles density-functional theory calculations with plane-wave basis sets and pseudopotential approximation were done to describe the structural, energetic, and electronic properties of sodium titanates considered in this study. All calculations were performed using the Vienna *ab initio* simulation package (VASP).[91,92] In this study, the PAW pseudopotentials and PW91 exchange-correlation functional were used in all of the calculations. Plane wave basis sets were used with a kinetic energy cutoff of 520 eV and an augmentation charge cutoff of 605.4 eV. The k-point sampling grids of $m \times n \times l$, obtained using the Monkhorst–Pack method,[93] are used for these bulk calculations, where m, n, and l are determined with a spacing of about 0.028 $Å^{-1}$ along the reciprocal axes of their unit cells. In the phonon calculations, a $4 \times 3 \times 2$ supercell of Na_2TiO_3, a $2 \times 2 \times 1$ supercell of $Na_4Ti_5O_{12}$, and a $2 \times 2 \times 2$ supercell of $Na_{16}Ti_{10}O_{18}$ were created from their optimized unit cells which were calculated through DFT. The displacement of 0.03 Å of nonequivalent atoms is generated. Then, for each supercell, the DFT calculations were performed again to obtain the force on each atom due to the displacements. These forces are carried back to PHONON package[94] to calculate the phonon dispersions and densities from which the partition function can be carried out.

dx.doi.org/10.1021/jp504922e | J. Phys. Chem. C 2014, 118, 19822−19832

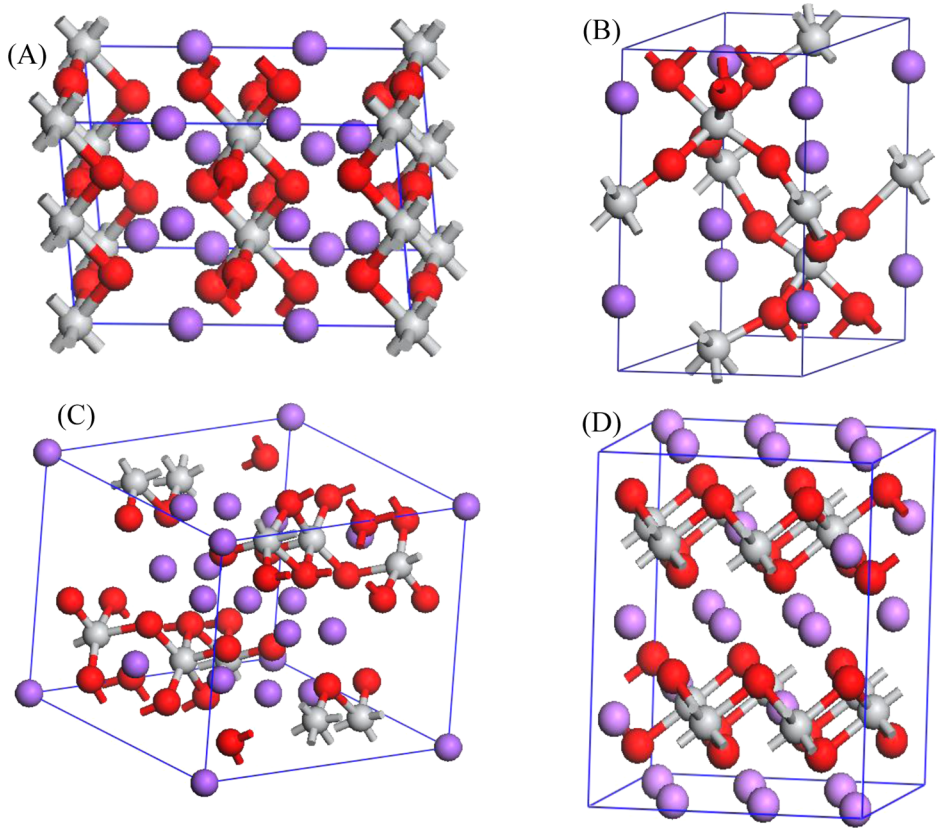

Figure 1. Crystal structures of different sodium titanates and sodium zirconate: (A) Na_2TiO_3 in space group *Immm* (No. 71), (B) $Na_4Ti_5O_{12}$ in space group *P*3 (No. 143), (C) $Na_{16}Ti_{10}O_{28}$ in space group $P\bar{1}$ (No. 2), and (D) Na_2ZrO_3 in space group *C*2/*c*1 (No. 15). Red stands for oxygen, purple stands for sodium, and gray stands for titanium or zirconium.

Table 1. Experimental and Optimized Crystal Structural Constants of Different Sodium Titanates and Sodium Zirconate. The Calculated Energy (E_{DFT}), the Zero-Point Energy (E_{zp}), and Entropy at T = 300 K Are Also Listed

crystal and space group	experiment	optimized and deviation (%)	E_{DFT} (eV/f.u.)	E_{zp} (kJ/mol)	Entropy (J/mol·K)
Na_2TiO_3	a = 9.535 Å	10.07599 (5.67%)	−39.01091	35.493	115.979
Immm (No. 71)[a]	b = 4.495 Å	4.22818 (−5.94%)			
Z = 2	c = 3.178 Å	3.01881 (−5.01%)			
$Na_4Ti_5O_{12}$	a = 5.31997 Å	5.35915 (0.74%)	−159.60844	129.348	409.775
*P*3 (No. 143)[b]	c = 9.5567 Å	9.63762 (0.85%)			
Z = 1	γ = 120°	120 (0%)			
$Na_{16}Ti_{10}O_{28}$	a = 10.51 Å	10.57946 (0.66%)	−371.65981	324.737	1072.428
$P\bar{1}$ (No. 2)[c]	b = 8.34 Å	8.39552 (0.67%)			
Z = 1	c = 8.53 Å	8.57695 (0.55%)			
	α = 112.63°	112.485 (−0.12%)			
	β = 104.1°	104.210 (0.11%)			
	γ = 102.19°	102.092 (−0.01%)			
Na_2ZrO_3	a = 5.63 Å	5.61281 (−0.18%)	−41.56924	34.497	119.319
*C*12/*c*1 (No. 15)[d]	b = 9.749 Å	9.73575 (−0.14%)			
Z = 8	c = 11.127 Å	10.95675 (−1.53%)			
	β = 99.98°	100.043 (0.01%)			

[a]From ref 95. [b]From ref 96. [c]From ref 97. [d]From ref 98.

III. RESULTS AND DISCUSSION

The crystal structures of Na-rich sodium titanates studied here are shown in Figure 1 and their experimental and optimized crystal parameters are listed in Table 1. As Liu et al.[86] reported, the Na_2TiO_3 has a NaCl-type structure with space group *Immm* (No. 71) as shown in Figure 1A. The other two Na-rich sodium titanates ($Na_4Ti_5O_{12}$ and $Na_{16}Ti_{10}O_{28}$) possess the following space groups P3 (No. 143) and $P\bar{1}$ (No. 2), and they are shown in Figure 1 panels B and C. For comparison reasons, the structure of Na_2ZrO_3 ($C_{12/c1}$ (No. 15) is also shown in Figure 1D and described in Table 1.

Na_2TiO_3 was synthesized via a solid state reaction, and the corresponding XRD pattern is shown in Figure 2. The XRD pattern fits very well with the 00-050-0110 PDF file, which

dx.doi.org/10.1021/jp504922e | J. Phys. Chem. C 2014, 118, 19822−19832

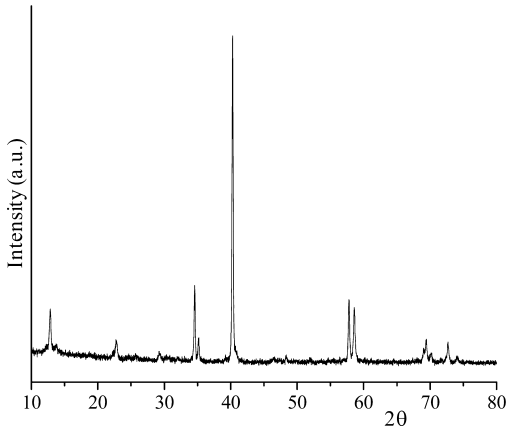

Figure 2. XRD pattern of the Na_2TiO_3 sample.

corresponds to the Na_2TiO_3 phase. After the structural identification, the N_2 adsorption−desorption isotherm and SEM analysis for the Na_2TiO_3 sample were acquired to determine some microstructural characteristics. Figure 3 shows

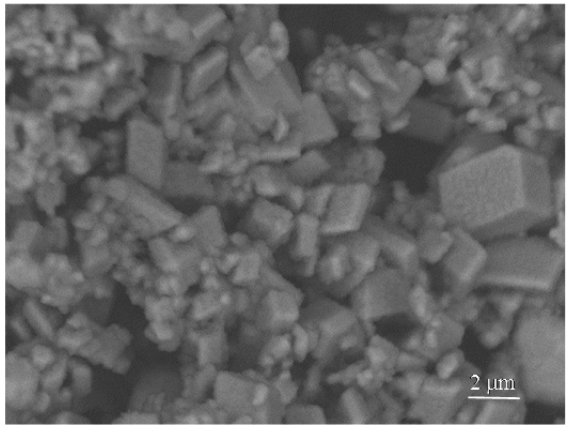

Figure 3. Backscattered electron image of the Na_2TiO_3 sample.

some of the morphological characteristics of the Na_2TiO_3 sample. Na_2TiO_3 sample formed well-defined polyhedral particles which varied their size from 200 to 300 nm up to 3−4 μm. These particles structured nondense agglomerates of 30−50 μm in size. To complement the Na_2TiO_3 microstructural characterization, it was analyzed by N_2 adsorption. The N_2 adsorption−desorption curve corresponds to a type II isotherm according to the IUPAC classification (data not shown). The isotherm did not present hysteresis. This behavior corresponds to a nonporous, dense aggregate of particles. Additionally, the surface area of the sample was estimated to be 0.8 m^2/g, using the BET model.

To further analyze and test this material, CO_2 chemisorption was studied. According to previous works based on sodium and lithium ceramics, a complete reaction between Na_2TiO_3 and CO_2 would be expected to follow the reaction 5:

$$Na_2TiO_3 + CO_2 \rightarrow Na_2CO_3 + TiO_2 \quad (5)$$

In fact, as it was described at the Introduction section, there is only one previous paper in which the CO_2 capture in Na_2TiO_3 was tested.[79] Unfortunately, in that paper the CO_2 capture process was only isothermally evaluated at 600 °C. Thus, the CO_2−Na_2TiO_3 system has not been totally analyzed as a function of temperature.

Figure 4 shows the dynamic thermogram of Na_2TiO_3 into a CO_2 flow. In this case, the thermogram did not present the

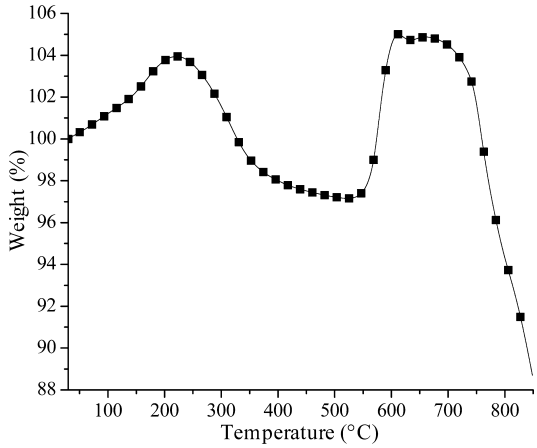

Figure 4. Dynamic thermogravimetric analysis of the Na_2TiO_3 sample into a CO_2 flux.

typical behavior observed for other lithium and sodium ceramics.[72,80] In this case, there is a continuous weight gain between 30 and 225 °C. The maximum weight increment observed at 225 °C was equal to 3.9 wt %. After that, between 230 and 524 °C the thermogram showed a weight decrement of 6.7 wt %. This means that the Na_2TiO_3 sample lost even more weight than that gained previously. Then, a sudden second weight increment was produced between 530 and 610 °C. Here, the total weight increment was equal to 8 wt %. After this weight increment, the weight did not vary until 700 °C, a temperature at which the weight began to decrease. In fact, the last weight decrement went up to only 88 wt % of the initial weight. In other words, the Na_2TiO_3 sample lost 12 wt %.

In general, lithium and sodium ceramics present one or two consecutive weight increments associated with the superficial and bulk CO_2 chemisorption process followed from a final weight increment, which is similar to the previously weight gained.[72,80] Only in some cases, a weight decrement between the two weight increments has been reported, and it has been associated with a superficial CO_2 chemisorption−desorption equilibrium.[75] In those cases, the weight decrement never was equal or higher than the initial weight increment. Nevertheless, in the Na_2TiO_3 case, both weight increments are associated with sequential weight decrements, which are higher than the previous increments. Hence, it seems that Na_2TiO_3 possesses a different CO_2 capture reaction mechanism, depending on temperature, and its thermal stability is not as high as in the ceramics previously reported. Therefore, different isothermal experiments were performed, and the products obtained from those isotherms were recharacterized by XRD, SEM, and TEM.

Figure 5 shows the Na_2TiO_3 isotherms obtained at different temperatures into a CO_2 flow. The initial isothermal experiment was performed at 250 °C, as the first maximum weight increment was at a similar temperature. This isotherm did not reach the equilibrium after 3 h and the weight increase was only 2.6 wt %. The second isotherm was performed at 400 °C, where the first weight decrement is significantly evidenced. This isotherm did not seem to present any important weight increment, as only less than 0.1 wt % of CO_2 was captured in

dx.doi.org/10.1021/jp504922e | J. Phys. Chem. C 2014, 118, 19822−19832

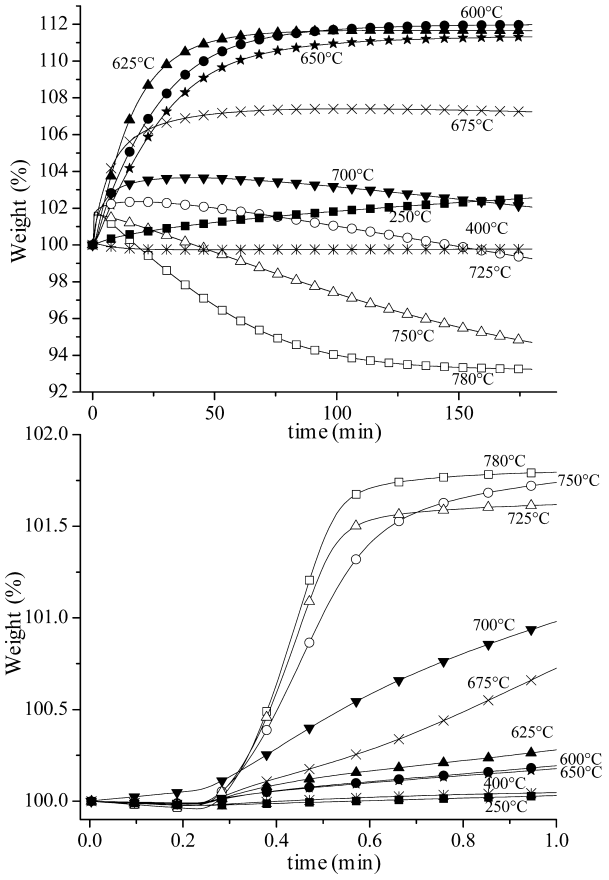

Figure 5. Na_2TiO_3–CO_2 chemisorption isotherms at different temperatures: complete isotherms (A) and first minute of the same isotherms (B).

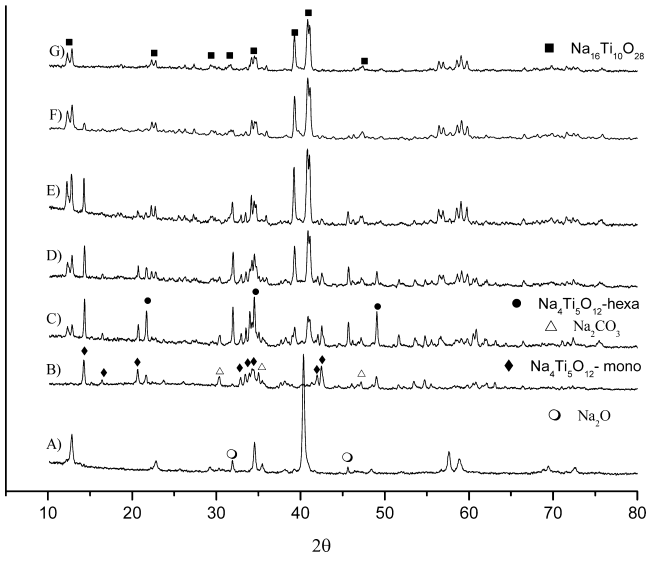

Figure 6. XRD patterns of the Na_2TiO_3–CO_2 products treated isothermally at different temperatures. (A) 250, (B) 650, (C) 675, (D) 700, (E) 725, (F) 750, (G) 780 °C.

the first seconds, but this CO_2 was immediately desorbed. Kinetically, the insipient CO_2 capture was faster at 400 °C than at 250 °C only during the first minute (Figure 5B). This behavior would be expected from the previous dynamic TG experiment. Between 600 and 650 °C isotherms presented the typical exponential behavior, gaining ∼11.5 wt % (efficiency of 40%). In fact the maximum weight increment (11.9 wt %) was observed at 600 °C, although the CO_2 chemisorption was faster at higher temperatures, up to 780 °C (Figure 5B). However, the isotherms performed between 675 and 780 °C decreased their final weights. At 675 and 700 °C the final weight increments were 7.2 and 2.0 wt % respectively, evidencing that a CO_2 chemisorption–desorption equilibrium was activated and favored as a function of temperature. Additionally, isotherms performed at T > 700 °C presented final weight decrements (wt % < 100%), although these isotherms presented weight increment during the first minutes. For example, the isotherm performed at 750 °C gained 1.6 wt % in the first 3 min, but after 3 h the isotherm final weight was equal to −5.3 wt %. Of course, these results clearly showed that not only CO_2 has been desorbed at high temperatures, but also part of the Na_2TiO_3 is being decomposed.

To elucidate the CO_2–Na_2TiO_3 chemisorption mechanism, as a function of temperature, the isothermal products were analyzed by XRD, SEM, and TEM. Figure 6 shows the XRD patterns of all CO_2–Na_2TiO_3 isothermal products, and a pristine Na_2TiO_3 pattern was included for comparison purposes. The 250 and 400 °C sample products evidenced the prevalence of the Na_2TiO_3 phase (00-050-0110 PDF file), as it could be expected. Nevertheless, new and well-defined peaks appeared at 27.5°, 31.8°, 45.6°, 56.5°, and 75.3° in 2θ. In fact, the intensity of these new peaks increased as a function of temperature. Sodium carbonate (Na_2CO_3) was not detected as the CO_2 chemisorption was almost negligible at these temperatures, but the new diffraction peaks fit to cubic sodium oxide phase (Na_2O, 96-900-9064 PDF file). Thus, in this temperature range 250–400 °C, CO_2 is initially chemisorbed on Na_2TiO_3, which must produce Na_2CO_3. However, CO_2 is desorbed after some minutes, leaving the sodium atoms as Na_2O over the Na_2TiO_3 particle surfaces. This relatively low temperature range (250–400 °C) must not allow the sodium diffusion, and its reincorporation into the Na_2TiO_3 phase. Moreover, the Na_2TiO_3 must tolerate a partial sodium extraction without being destabilized because of its layered crystalline structure.[83]

To complement the XRD results related to the Na_2O formation, SEM and TEM characterizations were performed. Figure 7 shows different morphological aspects of the Na_2TiO_3–CO_2 product obtained at 400 °C. In general, the morphology of this sample did not seem to present important variations in comparison to the original Na_2TiO_3 sample (see Figure 3), as it can be seen in the backscattered image (Figure 7A). The sample presented well-defined polyhedral particles of around 2–3 μm. However, the secondary electron image evidenced important changes in the Na_2TiO_3 particle surfaces (Figure 7B). It is clear that the Na_2TiO_3 sample formed a corrugated surface produced by the formation of tiny spherical-like structures. In fact, these spherical-like structures were confirmed through a TEM analysis (Figure 7C), where a particle size of ∼100 nm was determined. Of course, the formation of these nanoparticles should be related to the Na_2O formation, which was previously evidenced by XRD.

Coming back to the XRD results presented (Figure 6), the patterns corresponding to the isothermal products obtained between 600 and 780 °C showed the formation of different phases. As it could be expected, Na_2CO_3 was produced due to the CO_2 chemisorption. However, Na_2TiO_3 did not totally react according to eq 1, in which Na_2CO_3 and TiO_2 would be produced. Here, a different sodium titanate was produced,

dx.doi.org/10.1021/jp504922e | J. Phys. Chem. C 2014, 118, 19822–19832

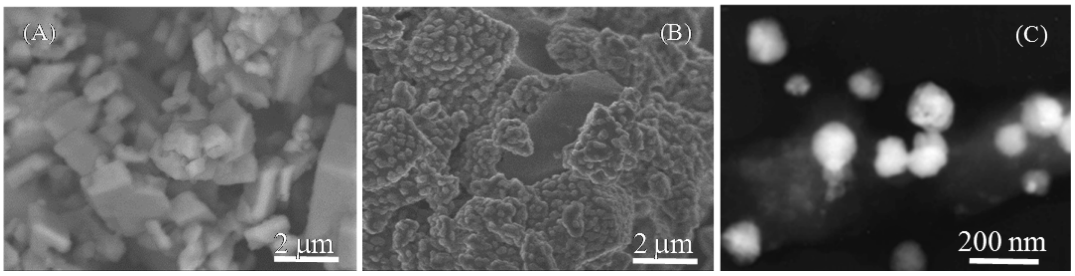

Figure 7. Electron microscope analysis of the Na_2TiO_3 sample treated at 400 °C into a CO_2 flux. Backscattered scanning electron (A), secondary scanning electron (B), and bright field transmission electron images (C).

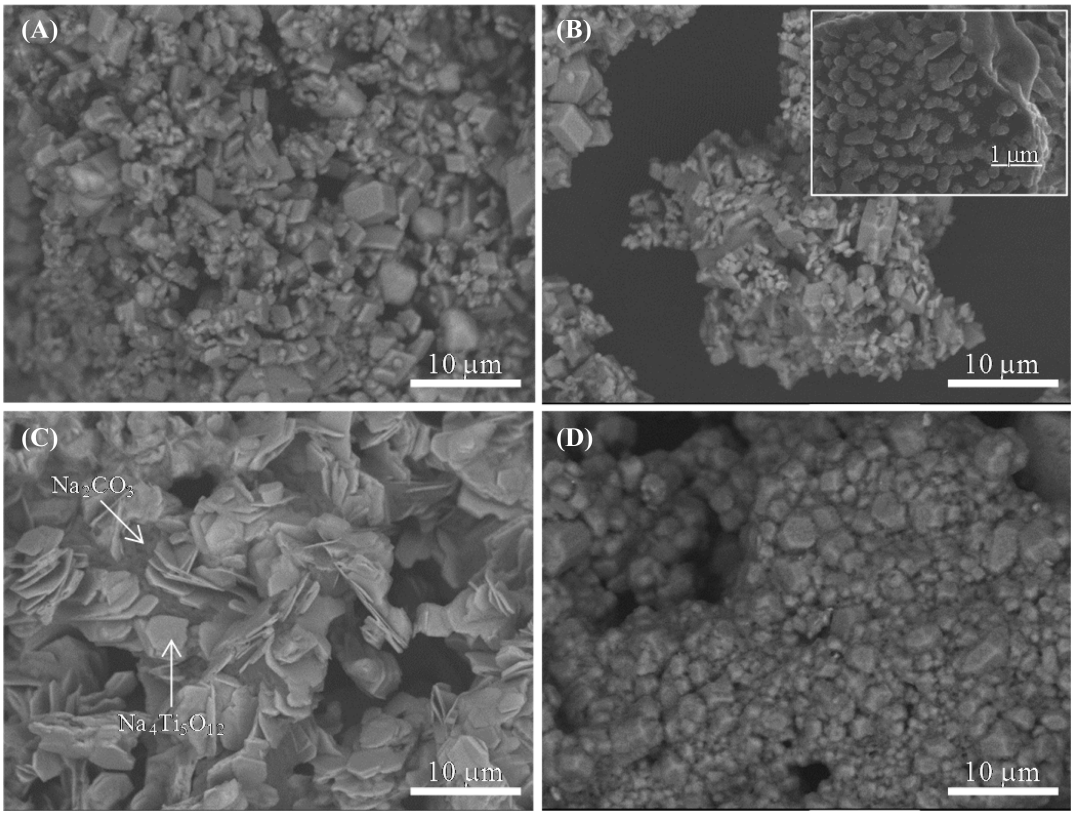

Figure 8. Scanning electron images of pristine Na_2TiO_3 (A) and Na_2TiO_3−CO_2 isothermal products obtained at 400 (B), 600 (C), and 750 °C (D).

$Na_4Ti_5O_{12}$. It means that Na_2TiO_3 only reacts partially with CO_2, in this temperature range (600−650 °C), according to the following reaction:

$$\frac{5}{3}Na_2TiO_3 + CO_2 \rightarrow Na_2CO_3 + \frac{1}{3}Na_4Ti_5O_{12} \quad (6)$$

Moreover, two other issues must be pointed out from these XRD patterns. The $Na_4Ti_5O_{12}$ crystalline phase changes from monoclinic to hexagonal, when temperature is increased from 650 to 675 °C and Na_2O appears at 675 °C. The $Na_4Ti_5O_{12}$ phase change can be related to different thermal stabilities. On the contrary, the Na_2O formation may be related to the CO_2 desorption process. However, at these temperatures sodium should not have diffusion problems to regenerate the Na_2TiO_3 phase, as it has been probed for other sodium ceramics, such as Na_2ZrO_3.[72] However, the secondary sodium titanate phase ($Na_4Ti_5O_{12}$) possesses a denser crystalline structure (2.2 g/cm^3) than Na_2TiO_3 (1.8 g/cm^3), which may inhibit the sodium diffusion and consequently the Na_2TiO_3 regeneration.

The crystal structures of these sodium titanates are quite different. In Na_2TiO_3, each Ti is coordinated with six oxygen atoms and each oxygen binds with two Ti atoms to form a TiO_3 plane (Figure 1A). Along the ⟨100⟩ direction, between $[TiO_3]$ planes, there are two Na layers interacting with the oxygen atoms of the $[TiO_3]$ planes. Interestingly, the crystal structure of Na_2TiO_3 is different with Na_2ZrO_3 as shown in Figure 1D. However, in the $Na_4Ti_5O_{12}$ structure (Figure 1B), each $[TiO_4]$ tetrahedral chain is surrounded by Na atoms, and in $Na_{16}Ti_{10}O_{28}$ (Figure 1C), each Ti coordinates with five oxygen atoms in which only one binds perpendicular with Ti of $[TiO_5]$, another two pair of oxygen atoms bind with two Ti of neighboring $[TiO_5]$ clusters. Obviously, different structures result in different electronic and thermodynamic properties.

At temperatures higher than 650 °C Na_2CO_3, $Na_4Ti_5O_{12}$, and Na_2O tended to disappear, while $Na_{16}Ti_{10}O_{28}$ appears as a function of temperature. Therefore, XRD patterns and isothermal results show that the CO_2−Na_2TiO_3 interaction is weakened if the temperature is increased. In fact, $Na_{16}Ti_{10}O_{28}$ was the only phase detected at 780 °C. The $Na_{16}Ti_{10}O_{28}$

dx.doi.org/10.1021/jp504922e | J. Phys. Chem. C 2014, 118, 19822−19832

formation could be explained by two different mechanisms. (1) If the quantity of sodium released from Na_2TiO_3 is reduced more than that observed at around 600−650 °C, the following reactions 7 and 8 may be established.

$$5Na_2TiO_3 + CO_2 \rightarrow Na_2CO_3 + \frac{1}{2}Na_{16}Ti_{10}O_{28} \quad (7)$$

where Na_2CO_3 decomposes immediately, as follows:

$$Na_2CO_3 \rightarrow CO_2 + Na_2O_{(sub)} \quad (8)$$

(2) On the contrary, if reaction 2 prevails, part of the sodium must sublime as Na_2O during CO_2 desorption, while the other part of the sodium atoms must be reincorporated to the $Na_4Ti_5O_{12}$ structure (reaction 9). In any case, Na_2O sublimation is proposed (reaction 8) based on the fact that $Na_{16}Ti_{10}O_{28}$ possesses a more similar density (2.05 g/cm^3) than does $Na_4Ti_5O_{12}$, which may have inhibited the Na_2TiO_3 total regeneration. It is confirmed as the final weight decreased more than 100 wt %, on those isotherms.

$$Na_2CO_3 + \frac{2}{5}Na_4Ti_5O_{12} \rightarrow \frac{1}{5}Na_2O_{(sub)} + CO_2 + \frac{1}{5}Na_{16}Ti_{10}O_{28} \quad (9)$$

The morphology evolution of the Na_2TiO_3−CO_2 system was followed by SEM. Figure 8 shows the backscattered images of the Na_2TiO_3 sample, for comparison purposes, and the Na_2TiO_3−CO_2 isothermal products obtained at 400, 600, and 750 °C. As it was previously described, the Na_2TiO_3 and the isothermal product of 400 °C presented similar particle sizes and shapes (Figure 8A,B). In fact, the only difference between these two samples was the superficial formation of the Na_2O spherical particles. However, the morphology varied significantly when the isotherm was performed at 600 °C. At this temperature, two different particles can be observed, some being flake-like particles surrounded by a dense matrix (Figure 8C). The presence of two different phases was determined by the particle contrasts observed in the corresponding back scattered electron images (BSEI), and they must correspond to Na_2CO_3 and $Na_4Ti_5O_{12}$, because they were the Na_2TiO_3 carbonation products detected by XRD. Thus, the contrast differences arise from the differences in mean atomic number ($\bar{Z}$) of Na_2CO_3 and $Na_4Ti_5O_{12}$, 8.666 and 11.904, respectively. Therefore, the back scattered electron coefficient (η) of these phases increases from 0.0999 to 0.1144 for Na_2CO_3 (dark phase) and $Na_4Ti_5O_{12}$ (light phase), respectively. Finally, the morphology of the 750 °C isothermal product ($Na_{16}Ti_{10}O_{28}$) presented very dense agglomerates composed of polyhedral particles of around 0.5−2 μm (Figure 8D). This morphology must have evolved from the original Na_2TiO_3 particles, which partially reacted with CO_2 producing $Na_{16}Ti_{10}O_{28}$, sublimating Na_2O, but mainly sintering.

Figures 9 and 10 show the calculated thermodynamic properties of CO_2 capture reactions by these sodium titanates. For comparison, the properties of Na_2ZrO_3 capture CO_2 are also presented in the same figures. It can be seen that there is a discrepancy between the Na_2TiO_3 calculated data reported here and the previously reported values fitted from HSC Chemistry database.[95] The differences arise from the initial structures used in each case. While the HSC reported value was measured with a Na_2O−TiO_2 mixture, the calculations in the present work were performed on the perfect crystal structure (*Immm*). In the

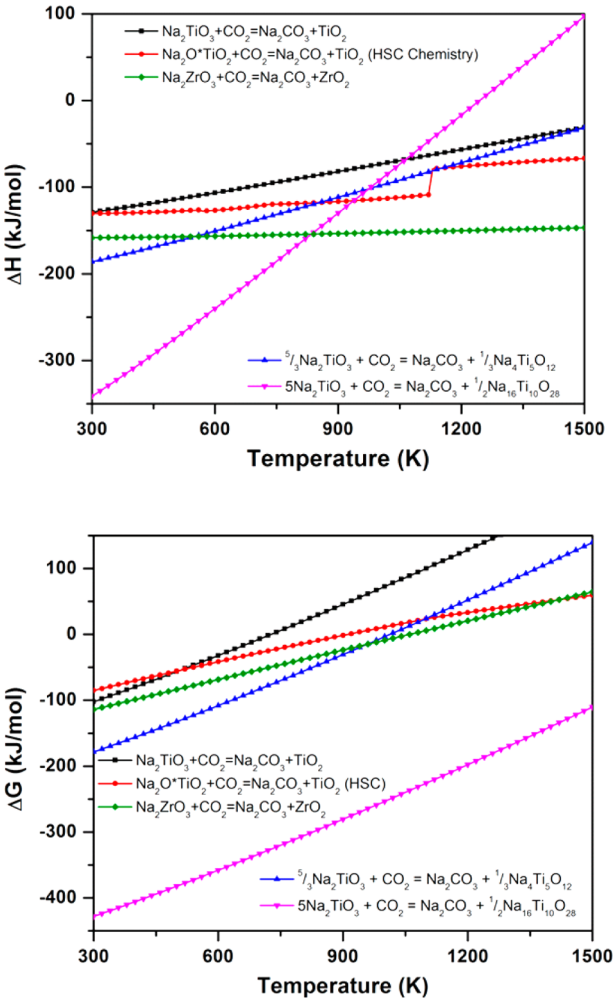

Figure 9. Calculated thermodynamic properties of CO_2 capture reactions by different sodium titanates and sodium zirconate.

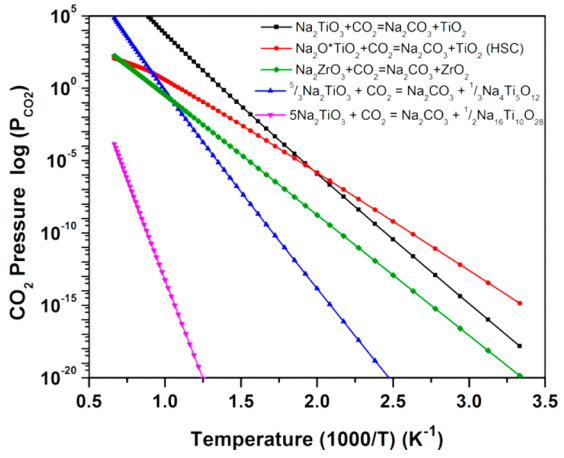

Figure 10. Calculated van't Hoff plots for reactions of sodium titanates and zirconate with CO_2.

phonon calculations, there are a few soft modes (negative frequency) which may cause some errors in evaluating thermodynamic properties and indicate phase deformation/change. As shown in Figure 9, when Na_2TiO_3 captures CO_2, producing TiO_2-rich sodium titanates ($Na_4Ti_5O_{12}$ and $Na_{16}Ti_{10}O_{28}$), the corresponding heat of reaction (ΔH) and

dx.doi.org/10.1021/jp504922e | J. Phys. Chem. C 2014, 118, 19822−19832

Table 2. Theoretical Weight Percentage of CO_2 Capture, The Energy Change (ΔE_{DFT}), and the Thermodynamic Properties (ΔH, ΔG, at T = 300 K)[a]

reaction	CO_2 absorbed (wt %)	ΔE_{DFT} (kJ/mol)	ΔH (T = 300 K) (kJ/mol)	ΔG (T = 300 K) (kJ/mol)	T_1 (K)	T_2 (K)	T_3 (K)
Na_2TiO_3+ CO_2 = Na_2CO_3 + TiO_2	31.24	−158.418	−128.917 (−130.367)[b]	−102.385 (−85.359)[b]	680	810	740
$5/3Na_2TiO_3$ + CO_2 = Na_2CO_3 + $1/3Na_4Ti_5O_{12}$	18.74	−234.443	−186.046	−178.411	945	1120	1020
$5Na_2TiO_3$ + CO_2 = Na_2CO_3 + $1/2Na_{16}Ti_{10}O_{28}$	6.25	−484.413	−341.321	−391.401	hT[c]	hT	hT
$Na_2O_{(sub)}$ + CO_2 = Na_2CO_{3c} [d]	70.99	−284.707	−282.372	−231.900	hT	hT	hT
$1/5Na_2O_{(sub)}$ + CO_2 + $1/5Na_{16}Ti_{10}O_{28}$ = Na_2CO_3 + $2/5Na_4Ti_5O_{12}$	16.22	−418.155	−303.309	−324.274	hT	hT	hT
Na_2ZrO_3 + CO_2 = Na_2CO_3 + ZrO_{2d} [e]	23.76	−140.684	−158.327	−114.121	925	1275	1065

[a]The turnover temperatures (T_1, T_2, T_3) of these CO_2 capture reactions under the conditions of post-combustion (P_{CO_2} = 0.1 bar), pre-combustion (P_{CO_2} = 20 bar), and P_{CO_2} = 1 bar are also listed. [b]From HSC Chemistry database 95. [c]hT means the temperature exceeds our temperature range (1500 K). [d]From ref 99. [e]From ref 98.

Gibbs free (ΔG) energies become more negative, resulting in higher turnover temperatures (Figure 10). However, the theoretical CO_2 capacity is reduced as it is summarized in Table 2.

To further analyze the isothermal curves presented in Figure 5, these data were fitted to a first-order reaction.[30,65,70] This model was selected as there are several processes involved in this reaction-mechanism, thus it was not possible to fit the data to multiple exponential models. However, during the first moments of the CO_2 chemisorption process, one can assume that a first-order reaction is taking place with respect to Na_2TiO_3 surface particles, as CO_2 was present in excess (60 mL/min). Therefore, the rate law can be assumed as follows:

$$\ln[Na_2TiO_3] = -kt \quad (10)$$

in which k is the reaction rate constant, t is the time, and $[Na_2TiO_3]$ is the molar concentration of the ceramic. As expected, data trends were linear only over very short intervals (60 s approximately), assuming a superficial Na_2TiO_3 carbonation reaction, and before any diffusion process or Na_2TiO_3 structural change are produced. The corresponding k values are presented in Table 3. k values tend to increase as a function of temperature. In addition, if these kinetic data are compared to similar k values, obtained for other alkaline ceramics, it can be seen that these values are lower than those reported for the Li_8SiO_6 and Na_2ZrO_3, among others.[30,70,74−76] Specifically, Na_2ZrO_3[70,74−76] reported k values between 1×10^{-3} and 2×10^{-2} s^{-1} at the optimum temperatures (600−700 °C), while the k values obtained with Na_2TiO_3, between 600 and 650 °C (the optimum temperature range), were around 1.7 and 2.5×10^{-4} s^{-1}. Thus, these results clearly show that CO_2 chemisorption on Na_2TiO_3 is slower than that on Na_2ZrO_3, although both sodium ceramics possess similar crystalline layered structures. This important difference may be related to variations observed on the structural evolution of each ceramic. While Na_2ZrO_3 evolves directly to Na_2CO_3 and ZrO_2, Na_2TiO_3 reacts only partially to produce Na_2CO_3 and different sodium titanates with lower Na:Zr molar ratios. So, sodium reactivity seems to be more limited on sodium titanate.

Table 3. First-Order Reaction Rate Constants of the Na_2TiO_3−CO_2 System at Different Temperatures

temperature (°C)	k (seg^{-1})
250	1.38×10^{-5}
400	5.53×10^{-5}
600	1.70×10^{-4}
625	2.48×10^{-4}
650	1.67×10^{-4}
675	5.55×10^{-4}
700	6.82×10^{-4}
725	2.40×10^{-3}
750	3.23×10^{-3}
780	3.57×10^{-3}

From Figure 10, a comparison of Na_2TiO_3 with Na_2ZrO_3 shows that, under the same CO_2 pressure, the turnover temperature for Na_2TiO_3 capturing CO_2 is lower than that of Na_2ZrO_3, as the latter reacting with CO_2 has more negative heat of reaction and Gibbs free energy with increasing temperatures. Likewise, if k values are dependent on temperature, the plot of ln k/T versus $1/T$ should produce a straight line according to Eyring's model, which is used for heterogeneous reactions (Figure 11) and allows a determination of the activation enthalpy ($\Delta H^{\ddagger}$). In the Na_2TiO_3−CO_2 system, two different $\Delta H^{\ddagger}$ trends were determined. Between 200 and 650 °C the $\Delta H^{\ddagger}$ value was 21.6 kJ/mol, while at higher temperatures (650−780 °C), it was equal to 188.1 kJ/mol. These results indicate that the CO_2 chemisorption in Na_2TiO_3 has a higher temperature dependence than those determined from other alkaline ceramics, such as Na_2ZrO_3 (33 kJ/mol).[75] It

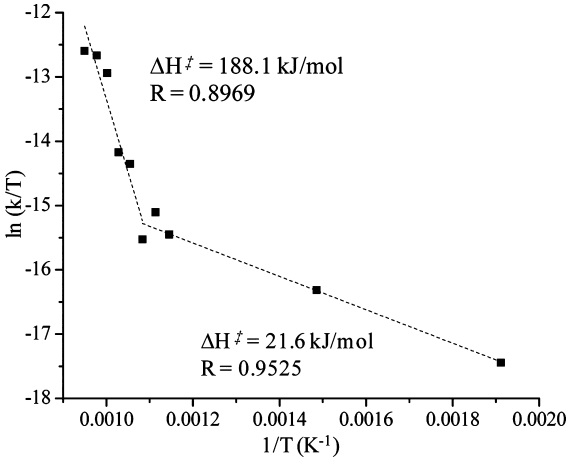

Figure 11. Eyring-type plot of ln k/T vs $1/T$ for data obtained assuming a first-order reaction of $[Na_2TiO_3]$ into a saturated CO_2 flux. Only the data obtained between 600 and 780 °C was considered for this analysis.

dx.doi.org/10.1021/jp504922e | J. Phys. Chem. C 2014, 118, 19822−19832

means that CO_2 chemisorption on Na_2TiO_3 is highly dependent on temperature.

From all these results, it can be established that CO_2 chemisorption on Na_2TiO_3 depends on different factors. Although CO_2 reacts with the Na_2TiO_3 particle surfaces as a function of temperature (kinetics results), the Na_2TiO_3 structural evolution seems to control the sodium accessibility and consequently the CO_2 chemisorption−desorption equilibrium. Sodium atoms seem to be partially extracted from the layered Na_2TiO_3 crystalline structure to react with CO_2, producing Na_2CO_3 and $Na_4Ti_5O_{12}$ or $Na_{16}Ti_{10}O_{28}$ depending on temperature.

IV. CONCLUSIONS

Na_2TiO_3 was synthesized via a solid state reaction. The sample structure and microstructure were analyzed using XRD, SEM, TEM, and N_2 adsorption. The CO_2 chemisorption capacity on Na_2TiO_3 was evaluated both dynamically and isothermally thermogravimetrically, in which the isothermal products were recharacterized using XRD, SEM, and TEM. Between 250 and 400 °C, CO_2 is initially chemisorbed on Na_2TiO_3, which must produce Na_2CO_3. However, CO_2 is desorbed after some minutes, leaving the sodium atoms as Na_2O (determined by XRD and TEM) over the Na_2TiO_3 particle surfaces. As the temperature is not very high, sodium seems not to be kinetically able to be reincorporated into the Na_2TiO_3 structure. Then, at higher temperatures (600−650 °C), the CO_2 chemisorption evolved to form different phases, Na_2CO_3 (produced due to the CO_2 chemisorption) and $Na_4Ti_5O_{12}$, in addition to Na_2O. Thus, the Na_2O formation may be related to a partial CO_2 desorption process. However, at $T \geq 650$ °C Na_2CO_3, $Na_4Ti_5O_{12}$, and Na_2O tended to disappear, while $Na_{16}Ti_{10}O_{28}$ is formed. In fact, $Na_{16}Ti_{10}O_{28}$ was the only phase detected at 780 °C.

The kinetic parameter values (k) obtained for the Na_2TiO_3−CO_2 reaction mechanism tend to increase as a function of temperature. In addition, the $\Delta H^{\ddagger}$ value is 140.9 kJ/mol between 600 and 780 °C. It means that CO_2 chemisorption on Na_2TiO_3 is highly dependent on temperature.

These results revealed that CO_2 chemisorption on Na_2TiO_3 depends on different factors. The Na_2TiO_3 structural evolution seems to be controlled by the sodium accessibility and consequently by the CO_2 chemisorption−desorption equilibrium. In fact at low temperatures Na_2O is produced due to an incomplete CO_2 chemisorption process. Later at higher temperatures Na_2TiO_3 reacts with CO_2 to produce Na_2CO_3 and $Na_4Ti_5O_{12}$ or $Na_{16}Ti_{10}O_{28}$ depending on the temperature range.

Additionally, all previous results were corroborated based on the theoretical thermodynamic data for the Na_2TiO_3−CO_2 reaction system, where different reaction products were estimated (TiO_2, $Na_4Ti_5O_{12}$, or $Na_{16}Ti_{10}O_{28}$). ΔE_{DFT}, ΔH, and ΔG values clearly showed the different thermal stability of each reaction process at different temperature ranges.

AUTHOR INFORMATION

Corresponding Author

*Tel.: +52(55)56224627. Fax: +52(55)56161371. E-mail: pfeiffer@iim.unam.mx

Notes

The authors declare no competing financial interest.

ACKNOWLEDGMENTS

This work was financially supported by the project SENER-CONACYT 150358. P. Sanchez-Camacho thanks CONACYT for financial support. The authors thank to Adriana Tejeda, Omar Novelo and Carlos Flores for technical help.

REFERENCES

(1) Zhao, Y.; Liu, X.; Yao, K. X.; Zho, L.; Han, Y. Superior Capture of CO_2 Achieved by Introducing Extra-framework Cations into N-doped Microporous Carbon. *Chem. Mater.* **2012**, *24*, 4725−4734.

(2) MacDowell, N.; Forin, N.; Buchard, A.; Hallett, J.; Galindo, A.; Jackson, G.; Adjiman, C. S.; Williams, C. K.; Shah, N.; Fennell, P. An Overview of CO_2 Capture Technologies. *Energy Environ. Sci.* **2010**, *3*, 1645−1669.

(3) Park, Y.; Decatur, J.; Lin, K. Y. A.; Park, A. H. Investigation of CO_2 Capture Mechanisms of Liquid-like Nanoparticle Organic Hybrid Materials via Structural Characterization. *Phys. Chem. Chem. Phys.* **2011**, *13*, 18115−18122.

(4) Yazadin, A. O.; Benin, A. I.; Faheem, S. A.; Jakubczak, P.; Low, J. J.; Willis, R. R.; Snurr, R. Q. Enhanced CO_2 Adsorption in Metal-Organic Frameworks via Occupation of Open-Metal Sites by Coordinated Water Molecules. *Chem. Mater.* **2009**, *21*, 1425−1430.

(5) Choi, S.; Dresse, J. H.; Jones, C. W. Adsorbent Materials for Carbon Dioxide Capture from Large Anthropogenic Point Sources. *ChemSusChem* **2009**, *2*, 796−854.

(6) Venegas, M. J.; Fregoso, E.; Escamilla, R.; Pfeiffer, H. Kinetic and Reaction Mechanism of CO_2 Sorption on Li_4SiO_4: Study of the Particle Size Effect. *Ind. Eng. Chem. Res.* **2007**, *46*, 2407−2412.

(7) Qi, Z.; Daying, H.; Yang, L.; Quian, Y.; Zibin, Z. Analysis of CO_2 Sorption/Desorption Kinetic Behaviors and Reaction Mechanisms on Li_4SiO_4. *AIChE J.* **2013**, *59*, 901−911.

(8) Mejía-Trejo, V. L.; Fregoso-Israel, E.; Pfeiffer, H. Textural, Structural, and CO_2 Chemisorption Effects Produced on the Lithium Orthosilicate by Its Doping with Sodium ($Li_{4-x}Na_xSiO_4$). *Chem. Mater.* **2008**, *20*, 7171−7176.

(9) Rodríguez-Mosqueda, R.; Pfieffer, H. Thermokinetic Analysis of the CO_2 Chemisorption on Li_4SiO_4 by Using Different Gas Flow Rates and Particle Sizes. *J. Phys. Chem. A* **2010**, *104*, 4535−4541.

(10) Seggiani, M.; Puccini, M.; Vitolo, S. High-Temperature and Low Concentration CO_2 Sorption on Li_4SiO_4 Based Sorbents: Study of the Used Silica and Doping Method Effects. *Int. J. Greenhouse Gas Control* **2011**, *5*, 741−748.

(11) Olivares-Marín, M.; Drage, T. C.; Maroto-Valer, M. M. Novel Lithium-Based Sorbents from Fly Ashes for CO_2 Capture at High Temperatures. *Int. J. Greenhouse Gas Control* **2010**, *4*, 623−629.

(12) Pacciani, R.; Torres, J.; Solsona, P.; Coe, C.; Quinn, R.; Hufton, J.; Golden, T.; Vega, L. F. Influence of the Concentration of CO_2 and SO_2 on the Absorption of CO_2 by a Lithium Orthosilicate-Based Absorbent. *Environ. Sci. Technol.* **2011**, *45*, 7083−7088.

(13) Duan, Y.; Parlinski, K. Density Functional Theory Study of the Structural, Electronic, Lattice Dynamical, and Thermodynamic Properties of Li_4SiO_4 and Its Capability for CO_2 Capture. *Phys. Rev. B* **2011**, *84*, 104113−1−104113−10.

(14) Ortiz-Landeros, J.; Gómez-Yáñez, C.; Pfeiffer, H. Surfactant-Assisted Hydrothermal Crystallization of Nanostructured Lithium Metasilicate (Li_2SiO_3) Hollow Spheres: II-Textural Analysis and CO_2-H_2O Sorption Evaluation. *J. Solid State Chem.* **2011**, *184*, 2257−2262.

(15) Quinn, R.; Kitzhoffer, R. J.; Hufton, J. R.; Golden, T. C. A High Temperature Lithium Orthosilicate-Based Solid Absorbent for Post Combustion CO_2 Capture. *Ind. Eng. Chem. Res.* **2012**, *51*, 9320−9327.

(16) Shan, S. Y.; Jia, Q. M.; Jiang, L. H.; Li, Q. C. Novel Li_4SiO_4-based Sorbents from Diatomite for High Temperature CO_2 Capture. *Ceram. Int.* **2013**, *39*, 5437−5441.

(17) Nair, B. N.; Burwood, R. P.; Goh, V. J.; Nakagawa, K.; Yamaguchi, T. Lithium Based Ceramic Materials and Membranes for High Temperature CO_2 Separation. *Prog. Mater. Sci.* **2009**, *54*, 511−541.

(18) Lee, S. J.; Yu, I. K.; Cho, S. Synthesis and Sintering Behavior of Li_4SiO_4 Fabricated by a PVA Polymer Solution Route. *J. Ceram. Proc. Res.* **2011**, *12*, 183−186.
(19) Xu, H.; Cheng, W.; Jin, X.; Wang, G.; Lu, H.; Wang, H.; Chen, D.; Fan, B.; Hou, T.; Zhang, R. Effect of the Particle Size of Quartz Powder on the Synthesis and CO_2 Absorption Properties of Li_4SiO_4 at High Temperature. *Ind. Eng. Chem. Res.* **2013**, *52*, 1886−1891.
(20) Wang, K.; Zhao, P.; Guo, X.; Han, D.; Chao, Y. High Temperature Capture of CO_2 on Li_4SiO_4-Based Sorbents from Biomass Ashes. *Environ. Prog. Sust. Ener.* DOI 10.1002/ep.11986.
(21) Seggiani, M.; Puccini, M.; Vitolo, S. Alkali-Promoted Lithium Orthosilicate for CO_2 Capture at High Temperature and Low Concentration. *Int. J. Greenhouse Gas Control* **2013**, *17*, 25−31.
(22) Wang, K.; Zhao, P.; Guo, X.; Li, Y.; Han, D.; Chao, Y. Enhancement of Reactivity in Li_4SiO_4-Based Sorbents from the Nano-sized Rice Husk Ash for High-Temperature CO_2 Capture. *Energy Convers. Mange.* **2014**, *81*, 447−454.
(23) Shan, S.; Jia, Q.; Jiang, L.; Wang, Y. Effect of Different Silicon Sources on CO_2 Absorption Properties of Li_4SiO_4 at High Temperature. *Adv. Mater. Res.* **2011**, *213*, 515−518.
(24) Nakagaki, T. Enhanced Hydrogen Production Process from Coal Integrated with CO_2 Separation Using Dual Chemical Looping. *Energy Procedia* **2011**, *4*, 324−332.
(25) Yamaguchi, T.; Nitsuma, T.; Nair, B. N.; Nakagawa, K. Lithium Silicate Based Membranes for High Temperature CO_2 Separation. *J. Membr. Sci.* **2007**, *294*, 16−21.
(26) Wang, K.; Guo, X.; Zhao, P.; Wang, F.; Zheng, C. High Temperature Capture of CO_2 on Lithium-Based Sorbents from Rice Husk Ash. *J. Hazard. Mater.* **2011**, *189*, 301−307.
(27) Romero-Ibarra, I. C.; Durán-Muñoz, F.; Pfeiffer, H. Influence of the K-, Na- and K-Na-carbonate Additions during the CO_2 Chemisorption on Lithium Oxosilicate (Li_8SiO_6). *Greenhouse Gases: Sci. Technol.* **2014**, *4*, 145−154.
(28) Romero-Ibarra, I. C.; Ortiz-Landeros, J.; Pfeiffer, H. Micro-structural and CO_2 Chemisorption Analyses of Li_4SiO_4: Effect of Surface Modification by the Ball Milling Process. *Thermochim. Acta* **2013**, *567*, 118−124.
(29) Duan, Y.; Pfeiffer, H.; Li, B.; Romero-Ibarra, I. C.; Sorescu, D. C.; Luebke, D. R.; Halley, J. W. CO_2 Capture Properties of Lithium Silicates with Different Ratios of Li_2O/SiO_2: An *ab initio* Thermodynamic and Experimental Approach. *Phys. Chem. Chem. Phys.* **2013**, *15*, 13538−13558.
(30) Durán-Muñoz, F.; Romero-Ibarra, I. C.; Pfeiffer, H. Analysis of the CO_2 Chemisorption Reaction Mechanism in Lithium Oxosilicate (Li_8SiO_6): A New Option for High-Temperature CO_2 Capture. *J. Mater. Chem. A* **2013**, *1*, 3919−3925.
(31) Ortiz-Landeros, J.; Romero-Ibarra, I. C.; Gómez-Yáñez, C.; Lima, E.; Pfeiffer, H. $Li_{4+x}(Si_{1-x}Al_x)O_4$ Solid Solution Mechanosynthesis and Kinetic Analysis of the CO_2 Chemisorption Process. *J. Phys. Chem. C* **2013**, *117*, 6303−6311.
(32) Chowdhury, M. B. I.; Quddus, M. R.; deLasa, H. I. CO_2 Capture with a Novel Solid Fluidizable Sorbent: Thermodynamics and Temperature Programmed Carbonation−Decarbonation. *Chem. Eng. J.* **2013**, *232*, 139−148.
(33) Shan, S. Y.; Jia, Q. M.; Jiang, L. H.; Li, Q. C.; Wang, Y. M.; Peng, J. H. Preparation and Kinetic Analysis of Li_4SiO_4 Sorbents with Different Silicon Sources for High Temperature CO_2 Capture. *Chin. Sci. Bull.* **2012**, *57*, 2475−2479.
(34) Shan, S. Y.; Li, S. M.; Jia, Q. M.; Jiang, L. H.; Wang, Y. M.; Peng, J. H. Impregnation Precipitation Preparation and Kinetic Analysis of Li_4SiO_4-Based Sorbents with Fast CO_2 Adsorption Rate. *Ind. Eng. Chem. Res.* **2013**, *52*, 6941−6945.
(35) Nakagawa, K.; Ohashi, T. A Novel Method of CO_2 Capture from High Temperature Gases. *J. Electrochem. Soc.* **1998**, *145*, 1344−1346.
(36) Pfeiffer, H.; Bosch, P. Thermal Stability and High-Temperature Carbon Dioxide Sorption on Hexa-lithium Zirconate ($Li_6Zr_2O_7$). *Chem. Mater.* **2005**, *17*, 1704−1710.
(37) Ida, J.; Xiong, R.; Lin, Y. S. Synthesis and CO_2 Sorption Properties of Pure and Modified Lithium Zirconate. *Separ. Purif. Technol.* **2004**, *36*, 41−51.
(38) Iwan, I.; Stephenson, H.; Ketchie, W. C.; Lapkin, A. High Temperature Sequestration of CO_2 Using Lithium Zirconates. *Chem. Eng. J.* **2009**, *146*, 249−258.
(39) Pannocchia, G.; Puccini, M.; Seggiani, M.; Vitolo, S. Experimental and Modeling Studies on High-Temperature Capture of CO_2 Using Lithium Zirconate Based Sorbents. *Ind. Eng. Chem. Res.* **2007**, *46*, 6696−6706.
(40) Ochoa-Fernández, E.; Rusten, H. K.; Jakobsen, H. A.; Rønning, M.; Holmen, A.; Chen, D. Sorption Enhanced Hydrogen Production by Steam Methane Reforming Using Li_2ZrO_3 as Sorbent: Sorption Kinetics and Reactor Simulation. *Catal. Today* **2005**, *106*, 41−46.
(41) Ochoa-Fernández, E.; Rønning, M.; Grande, T.; Chen, D. Nanocrystalline Lithium Zirconate with Improved Kinetics for High-Temperature CO_2 Capture. *Chem. Mater.* **2006**, *18*, 1383−1385.
(42) Ochoa-Fernández, E.; Rønning, M.; Yu, X.; Grande, T.; Chen, D. Compositional Effects of Nanocrystalline Lithium Zirconate on Its CO_2 Capture Properties. *Ind. Eng. Chem. Res.* **2008**, *47*, 434−442.
(43) Xiong, R.; Ida, J.; Lin, Y. S. Kinetics of Carbon Dioxide Sorption on Potassium-Doped Lithium Zirconate. *Chem. Eng. Sci.* **2003**, *58*, 4377−4385.
(44) Xiao, Q.; Tang, X.; Liu, Y.; Zhong, Y.; Zhu, W. Citrate Route to Prepare K-Doped Li_2ZrO_3 Sorbents with Excellent CO_2 Capture Properties. *Chem. Eng. J.* **2011**, *174*, 231−235.
(45) Xiao, Q.; Tang, X.; Liu, Y.; Zhong, Y.; Zhu, W. Comparison Study on Strategies to Prepare Nanocrystalline Li_2ZrO_3-Based Absorbents for CO_2 Capture at High Temperature. *Front. Chem. Sci. Eng.* **2013**, *7*, 297−302.
(46) Yin, X. S.; Zhang, Q. H.; Yu, J. G. Three-Step Calcination Synthesis of High-Purity Li_8ZrO_6 with CO_2 Absorption Properties. *Inorg. Chem.* **2011**, *50*, 2844−2850.
(47) Yin, X. S.; Song, M.; Zhang, Q. H.; Yu, J. G. High-Temperature CO_2 Capture on $Li_6Zr_2O_7$: Experimental and Modeling Studies. *Ind. Eng. Chem. Res.* **2010**, *49*, 6593−6598.
(48) Martínez-dlCruz, L.; Pfeiffer, H. Toward Understanding the Effect of Water Sorption on Lithium Zirconate (Li_2ZrO_3) during Its Carbonation Process at Low Temperatures. *J. Phys. Chem. C* **2010**, *114*, 9453−9458.
(49) Martínez-dlCruz, L.; Pfeiffer, H. Effect of Oxygen Addition on the Thermokinetic Properties of CO_2 Chemisorption on Li_2ZrO_3. *Ind. Eng. Chem. Res.* **2010**, *49*, 9038−9042.
(50) Radfarnia, H. R.; Iliuta, M. C. Surfactant-Template/Ultrasound-Assisted Method for the Preparation of Porous Nanoparticle Lithium Zirconate. *Ind. Eng. Chem. Res.* **2011**, *50*, 9295−9305.
(51) Yin, X. S.; Li, S. P.; Zhang, Q. H.; Yu, J. G. Synthesis and CO_2 Adsorption Characteristics of Lithium Zirconates with High Lithia Content. *J. Am. Ceram. Soc.* **2010**, *93*, 2837−2842.
(52) Xiao, Q.; Tang, X.; Zhang, Y.; Zhu, W. A Facile Starch-Assisted Sol−Gel Method to Synthesize K-Doped Li_2ZrO_3 Sorbents with Excellent CO_2 Capture Properties. *J. Am. Ceram. Soc.* **2012**, *95*, 1544−1548.
(53) Xiao, Q.; Liu, Y.; Zhong, Y.; Zhu, W. A Citrate Sol−Gel Method to Synthesize Li_2ZrO_3 Nanocrystals with Improved CO_2 Capture Properties. *J. Mater. Chem.* **2011**, *21*, 3838−3842.
(54) Wang, S.; An, C.; Zhang, Q. Syntheses and Structures of Lithium Zirconates for High-Temperature CO_2 Absorption. *J. Mater. Chem. A* **2013**, *1*, 3540−3550.
(55) Khokhani, M.; Khomane, R. B.; Kulkarni, B. D. Sodium-Doped Lithium Zirconate Nano Squares: Synthesis, Characterization and Applications for CO_2 Sequestration. *J. Sol-Gel Sci. Technol.* **2012**, *61*, 316−320.
(56) Kang, S. Z.; Wu, T.; Li, X.; Mu, J. Low Temperature Biomimetic Synthesis of the Li_2ZrO_3 Nanoparticles Containing $Li_6Zr_2O_7$ and High Temperature CO_2 Capture. *Mater. Lett.* **2010**, *64*, 1404−1406.
(57) Duan, Y. Structural and Electronic Properties of Li_8ZrO_6 and its CO_2 Capture Capabilities: An *ab initio* Thermodynamic Approach. *Phys. Chem. Chem. Phys.* **2013**, *15*, 9752−9760.

(58) Olivares-Marín, M.; Castro-Díaz, M.; Drage, T. C.; Maroto-Valer, M. M. Use of Small-Amplitude Oscillatory Shear Rheometry To Study the Flow Properties of Pure and Potassium-Doped Li_2ZrO_3 Sorbents During the Sorption of CO_2 at High Temperatures. *Sep. Purif. Technol.* **2010**, *73*, 415−420.
(59) Raskar, R.; Rane, V.; Gaikwad, A. The Applications of Lithium Zirconium Silicate at High Temperature for the Carbon Dioxide Sorption and Conversion to Syn-gas. *Water Air Soil Pollut.* **2013**, *224*, 1569−1583.
(60) Ávalos-Rendón, T.; Casa-Madrid, J.; Pfeiffer, H. Thermochemical Capture of Carbon Dioxide on Lithium Aluminates ($LiAlO_2$ and Li_5AlO_4): A New Option for the CO_2 Absorption. *J. Phys. Chem. A* **2009**, *113*, 6919−6923.
(61) Ávalos-Rendón, T.; Lara, V. H.; Pfeiffer, H. CO_2 Chemisorption and Cyclability Analyses of Lithium Aluminate Polymorphs (α- and β-Li_5AlO_4). *Ind. Eng. Chem. Res.* **2012**, *51*, 2622−2630.
(62) Ávalos-Rendón, T.; Pfeiffer, H. High CO_2 Chemisorption in α-Li_5AlO_4 at Low Temperatures (30−80 °C): Effect of the Water Vapor Addition. *Energy Fuels* **2012**, *26*, 3110−3114.
(63) Tilekar, G.; Shinde, K.; Kale, K.; Raskar, R.; Gaikwad, A. The Capture of Carbon Dioxide by Transition Metal Aluminates, Calcium Aluminate, Calcium Zirconate, Calcium Silicate and Lithium Zirconate. *Front. Chem. Sci. Eng.* **2011**, *5*, 477−491.
(64) Rodríguez-Mosqueda, R.; Pfeiffer, H. High CO_2 Capture in Sodium Metasilicate (Na_2SiO_3) at Low Temperatures (30−60 °C) through the CO_2−H_2O Chemisorption Process. *J. Phys. Chem. C* **2013**, *117*, 13452−13461.
(65) Palacios-Romero, L. M.; Lima, E.; Pfeiffer, H. Structural Analysis and CO_2 Chemisorption Study on Nonstoichiometric Lithium Cuprates ($Li_{2+x}CuO_{2+x/2}$). *J. Phys. Chem. A* **2009**, *113*, 193−198.
(66) Palacios-Romero, L. M.; Pfeiffer, H. Lithium Cuprate (Li_2CuO_2): A New Possible Ceramic Material for CO_2 Chemisorption. *Chem. Lett.* **2008**, *37*, 862−863.
(67) Matsukura, Y.; Okumura, T.; Kobayashi, R.; Oh-ishi, K. Synthesis and CO_2 Absorption Properties of Single-phase Li_2CuO_2 as a CO_2 Absorbent. *Chem. Lett.* **2010**, *39*, 966−967.
(68) Oh-ishi, K.; Matzukura, Y.; Okumura, T.; Matsunaga, Y.; Kabayashi, R. Fundamental Research on Gas−Solid Reaction between CO_2 and Li_2CuO_2 Linking Application for Solid CO_2 Absorbent. *J. Solid State Chem.* **2014**, *211*, 162−169.
(69) Zhao, T.; Ochoa-Fernández, E.; Rønning, M.; Chen, D. Preparation and High-Temperature CO_2 Capture Properties of Nanocrystalline Na_2ZrO_3. *Chem. Mater.* **2007**, *19*, 3294−3301.
(70) Alcérreca-Corte, I.; Fregoso-Israel, E.; Pfeiffer, H. CO_2 Absorption on Na_2ZrO_3: A Kinetic Analysis of the Chemisorption and Diffusion Processes. *J. Phys. Chem. C* **2008**, *112*, 6520−6525.
(71) Pfeiffer, H.; Vazquez, C.; Lara, V. H.; Bosch, P. Thermal Behavior and CO_2 Absorption of $Li_{2-x}Na_xZrO_3$ Solid Solutions. *Chem. Mater.* **2007**, *19*, 922−926.
(72) Martínez-dlCruz, L.; Pfeiffer, H. Microstructural Thermal Evolution of the Na_2CO_3 Phase Produced during a Na_2ZrO_3−CO_2 Chemisorption Process. *J. Phys. Chem. C* **2012**, *116*, 9675−9680.
(73) Ochoa-Fernández, E.; Rønning, M.; Yu, X.; Grande, T.; Chen, D. Compositional Effects of Nanocrystalline Lithium Zirconate on Its CO_2 Capture Properties. *Ind. Eng. Chem. Res.* **2008**, *47*, 434−442.
(74) Martínez-dlCruz, L.; Pfeiffer, H. Cyclic CO_2 Chemisorption−Desorption Behavior of Na_2ZrO_3: Structural, Microstructural and Kinetic Variations Produced as a Function of Temperature. *J. Solid State Chem.* **2013**, *204*, 298−304.
(75) Alcántar-Vázquez, B.; Diaz, C.; Romero-Ibarra, I. C.; Lima, E.; Pfeiffer, H. Formation of Sodium Titanate Nanotube Films by Hydrothermal Transcription. *J. Phys. Chem. C* **2013**, *117*, 16483−16491.
(76) Sánchez-Camacho, P.; Romero-Ibarra, I. C.; Pfeiffer, H. Thermokinetic and Microstructural Analyses of the CO_2 Chemisorption on K_2CO_3−Na_2ZrO_3. *J. CO_2 Util.* **2013**, *3*−*4*, 14−20.
(77) Zhao, T.; Rønning, M.; Chen, D. Preparation of Nanocrystalline Na_2ZrO_3 for High-Temperature CO_2 Acceptors: Chemistry and Mechanism. *J. Energy Chem.* **2013**, *22*, 387−393.
(78) Radfarnia, H. R.; Iliuta, M. C. Application of Surfactant-Template Technique for Preparation of Sodium Zirconate as High Temperature CO_2 Sorbent. *Sep. Purif. Technol.* **2012**, *93*, 98−106.
(79) López-Ortiz, A.; Perez-Rivera, N. G.; Reyes-Rojas, A.; Lardizabal-Gutierrez, D. Novel Carbon Dioxide Solid Acceptors Using Sodium Containing Oxides. *Sep. Sci. Technol.* **2004**, *39*, 3559−3572.
(80) Ortiz-Landeros, J.; Ávalos-Rendón, T.; Gómez-Yáñez, C.; Pfeiffer, H. Analysis and Perspectives Concerning CO_2 Chemisorption on Lithium Ceramics Using Thermal Analysis. *J. Therm. Anal. Calorim.* **2012**, *108*, 647−655.
(81) Meng, X. D.; Wang, D. Z.; Liu, J. H.; Zhang, S. Y. Preparation and Characterization of Sodium Titanate Nanowires from Brookite Nanocrystallites. *Mater. Res. Bull.* **2004**, *39*, 2163−2170.
(82) Yada, M.; Inoue, Y.; Uota, M.; Torikai, T.; Watari, T.; Noda, I.; Hotokebuchi, T. Formation of Sodium Titanate Nanotube Films by Hydrothermal Transcription. *Chem. Mater.* **2008**, *20*, 364−366.
(83) Mao, S. Y.; Ren, X. X.; Zhou, Z. H. Synthesis and Crystal Structure of Na_2TiO_3. *Chin. J. Struct. Chem.* **2008**, *27*, 553.
(84) Kaneko, H.; Hosokawa, Y.; Kojima, N.; Gokon, N.; Haegawa, N.; Kitamura, M.; Tamaura, Y. Studies on Metal Oxides Suitable for Enhancement of the O_2-Releasing Step in Water Splitting by the $MnFe_2O_4$−Na_2CO_3. *Energy* **2001**, *26*, 919−929.
(85) Marciniuk, L. L.; Hammer, P.; Pastore, H. O.; Schuchardt, U.; Cardoso, D. Sodium Titanate as Basic Catalyst in Transesterification Reactions. *Fuel* **2014**, *118*, 48−54.
(86) Liu, Y. H.; Zhao, W.; Wang, W. J.; Yang, X.; Chu, J. L.; Xue, T. Y.; Qi, T.; Wu, J. Y.; Wang, C. R. Study on the Transformation from NaCl-type Na_2TiO_3 to Layered Titanate. *J. Phys. Chem. Solids* **2012**, *73*, 402−406.
(87) Duan, Y.; Sorescu, D. C. Density Functional Theory Studies of the Structural, Electronic, and Phonon Properties of Li_2O and Li_2CO_3: Application to CO_2 Capture Reaction. *Phys. Rev. B* **2009**, *79*, 014301.
(88) Duan, Y.; Sorescu, D. C. CO_2 Capture Properties of Alkaline Earth Metal Oxides and Hydroxides: A Combined Density Functional Theory and Lattice Phonon Dynamics Study. *J. Chem. Phys.* **2010**, *133*, 074508.
(89) Zhang, B.; Duan, Y.; Johnson, J. K. Density Functional Theory Study of CO_2 Capture with Transition Metal Oxides and Hydroxides. *J. Chem. Phys.* **2012**, *136*, 064516.
(90) Chase, M. W. J. NIST-JANAF Themochemical Tables, 4th edition. *J. Phys. Chem. Ref. Data*, Monograph **1998**, *9*, 1−1951.
(91) Kresse, G.; Hafner. Ab Initio Molecular Dynamics for Liquid Metals. J. *Phys. Rev. B* **1993**, *47*, 558−561.
(92) Kresse, G.; Furthmuller, J. Efficiency of Ab-Initio Total Energy Calculations for Metals and Semiconductors Using a Plane-Wave Basis Set. *Comput. Mater. Sci.* **1996**, *6*, 15−50.
(93) Monkhorst, H. J.; Pack, J. D. Special Points for Brillouin-Zone Integrations. *Phys. Rev. B* **1976**, *13*, 5188−5192.
(94) Parlinski, K. *PHONON*; Computing for Materials: Krakow, Poland, 2006
(95) *HSC Chemistry*, version 6.1; Outotec Research Oy: Pori, Finland, 2006; www.outotec.com/hsc.
(96) Avdeev, M.; Kholkin, A. Low-Temperature $Na_4Ti_5O_{12}$ from X-ray and Neutron Powder Diffraction Data. *Acta Crystall. C* **2000**, *56*, E539−E540.
(97) Mayer, M.; Perez, G. *Rev. Chim. Miner.* **1976**, *13*, 237.
(98) Duan, Y. A First-Principles Density Functional Theory Study of the Electronic Structural and Thermodynamic Properties of M_2ZrO_3 and M_2CO_3 (M = Na, K) and their Capabilities for CO_2 Capture. *J. Renew. Sustain. Energy* **2012**, *4*, 013109.
(99) Duan, Y.; Zhang, B.; Sorescu, D. C.; Johnson, J. K. CO_2 Capture Properties of M−C−O−H (M = Li, Na, K) Systems: A Combined Density Functional Theory and Lattice Phonon Dynamics Study. *J. Solid State Chem.* **2011**, *184*, 304−311.